Nonvolatile Multilevel States in Multiferroic Tunnel Junctions

Mei Fang,[1,2,*] Sangjian Zhang,[1] Wenchao Zhang,[1] Lu Jiang,[3] Eric Vetter,[4] Ho Nyung Lee,[3] Xiaoshan Xu,[5,†] Dali Sun,[4,‡] and Jian Shen[2,§]

[1]*Hunan Key Laboratory of Super Microstructure and Ultrafast Process, School of Physics and Electronics, Central South University, Changsha, Hunan 410083, China*
[2]*State Key Laboratory of Surface Physics and Department of Physics and Collaborative Innovation Center of Advanced Microstructure, Fudan University, Shanghai 200433, China*
[3]*Materials Science and Technology Division, Oak Ridge National Laboratory, Oak Ridge, Tennessee 37831, USA*
[4]*Department of Physics, North Carolina State University, Raleigh, North Carolina 27695, USA*
[5]*Department of Physics and Astronomy, Nebraska Center for Materials and Nanoscience, University of Nebraska, Lincoln, Nebraska 68588, USA*

(Received 4 April 2019; revised manuscript received 1 July 2019; published 22 October 2019)

Manipulation of tunneling spin-polarized electrons via a ferroelectric interlayer sandwiched between two ferromagnetic electrodes, dubbed multiferroic tunnel junctions (MFTJs), can be achieved not only by the magnetic alignment of two ferromagnets, but also by the electric polarization of the ferroelectric interlayer; this provides great opportunities for next-generation multistate memory devices. Here, we show that a $La_{0.67}Sr_{0.33}MnO_3$(LSMO)/$PbZr_{0.2}Ti_{0.8}O_3$(PZT)/Co structured MFTJ device can exhibit multilevel resistance states in the presence of gradually reversed ferroelectric domains via tunneling electroresistance and tunneling magnetoresistance, respectively. Nonvolatile ferroelectric control in the MFTJ can be attributed to separate contributions that arise from two independent ferroelectric channels in the PZT interlayer with opposite polarization. Our study shows the dominant role of "mixed" ferroelectric states on achieving accumulative electrical modulation of multilevel resistance states in MFTJs; thus paving the way for multifunctional device applications.

DOI: 10.1103/PhysRevApplied.12.044049

I. INTRODUCTION

Multiferroic tunnel junctions (MFTJs), consisting of two ferromagnetic (FM) electrodes separated by a thin ferroelectric (FE) insulating layer, have garnered great interests for potential multifunctional applications in the field of spintronics, as a result of their switchable electric polarization with high tunability [1]. By switching the electric polarization of the FE layer, the resistance of the MFTJ changes in accordance with the electrostatic effect, strain effect, interface effect, and so forth. [2]. This is demonstrated through tunnel electroresistance (TER), which can be described by the Brinkman model using the barrier height of the insulator and the screening length of the electrodes [3–5]. The change in resistance scales with the fraction of ferroelectric polarization domains, from which a parallel conduction model of ferroelectric poled-up and -down domains has been proposed [6]. A similar large TER effect has been reported in a semiconductor-based tunnel junction with an additional Schottky barrier on the semiconductor surface; this demonstrates the electrical modulation of both the height and the width of the barrier using ferroelectricity [7,8].

Owing to the adjacent FM electrodes attached to the FE material, the tunneling resistance of the MFTJ can be tuned by applying an external magnetic field, dubbed tunneling magnetoresistance (TMR) [9]. The pronounced magnetoelectric coupling (MEC) at the FM-FE interface enables us to actively manipulate the magnetic properties of the FM electrodes by switching the polarity of the FE interlayer, including the interfacial magnetism [10,11], magnetic anisotropy [12,13], spin polarization [14], magnetic domain size [15], its phase transition [16,17], among others [1,18–20]. This leads to the electrically modulated TMR response (e.g., polarity and magnitude) in MFTJs by switching the polarity of the FE interlayer [21–23]. By utilizing a ferroelectric material as the tunnel barrier layer, the MFTJs posses an additional degree of freedom to modulate spin transport and spin injection by electrical means, which is ideally desirable for chip integration. These magnetoelectric functionalities are employed for multifunctional spintronic devices, such as four-state memories [24–26]; thus making ferroelectric materials promising candidates for computing technologies.

*meifang@csu.edu.cn
†xiaoshan.xu@unl.edu
‡dsun4@ncsu.edu
§shenj5494@fudan.edu.cn

Here, we demonstrate that electrical control of both tunneling electro- and magnetoresistance can be achieved in one MFTJ device [i.e., $La_{0.67}Sr_{0.33}MnO_3$(LSMO)/$PbZr_{0.2}Ti_{0.8}O_3$(PZT)/Co] using ferroelectricity. The fabricated device exhibits multilevel nonvolatile resistance states by accumulatively tuning the area fraction of the ferroelectric up and down domains in the PZT interlayer. The correlated TER and TMR states at the "mixed" FE state are calculated using a two-channel parallel resistance circuit. Our work presents promising ferroelectric control of spin-dependent electron tunneling resistance in MFTJs towards next-generation bioinspired neuromorphic computing applications.

II. EXPERIMENTAL METHODS

Pulsed laser deposition (PLD) is used to grow 30 nm LSMO and then 5 nm PZT films epitaxially on the surface of a $SrTiO_3$ (STO) substrate. The topography and ferroelectric properties of the LSMO/PZT films are characterized by a Veeco Dimension 3100 piezoresponse force microscope (PFM) at room temperature, with atomically flat surfaces and switchable electric polarization [27]. Patterned 10-nm-thick Co layers and Au capping layers of around 10 nm are deposited on top of the LSMO/PZT films by thermal evaporation in a high-vacuum chamber (base vacuum $<1\times10^{-6}$ Pa) using a shadow mask to fabricate junctions with areas of $200\times250\ \mu m^2$. The magnetic properties of the LSMO films and the junctions are characterized by using a Quantum Design superconducting quantum interference device (SQUID). A Keithley 2400 source meter and physical property measurement system (PPMS, Quantum Design) are used for charge and spin transport measurements with controllable magnetic field and temperature. For electrical nonvolatile control of TER and TMR, a preset voltage bias (V_{max}) is programmed by ramping the voltage from zero to a certain level to initialize the accumulative ferroelectric state of the PZT interlayer in the presence of x poled-down FE domains ($0\%\le x\le100\%$). The TER and TMR effects are determined by measuring the resistance of the device at a small voltage bias, V_{MR} ($|V_{MR}|\le|V_{max}|$) as a function of electric field (R-V curves for the TER effect) and magnetic field (R-H curves for the TMR effect), respectively.

III. RESULTS AND DISCUSSION

A. TER characterization in MFTJs

A schematic diagram of the MFTJs is shown in Fig. 1(a). LSMO and Co films are used as ferromagnetic electrodes for spin-injection and detection. The magnetic hysteresis loops of the FM films are presented in Fig. 1(b), showing different coercive fields of about 40 and 500 Oe for the LSMO and Co, respectively. The parallel and antiparallel magnetic alignments of the FM electrodes in MFTJs are achieved by sweeping the magnetic field. The ferroelectric tunnel barrier comprises a 5-nm PZT film with switchable FE polarization. The FE polarization direction for an as-grown PZT film is pointing up. The reversal of the FE domain in this ultrathin PZT layer (i.e., from up to down) is demonstrated by applying a positive voltage bias through the PFM tip (>+0.8 V) [27–29], and is not expected to be affected by the top electrode [30]; this suggests similar FE switching behavior in the MFTJ configuration. The tunneling behavior of the MFTJ in the parallel magnetic configuration is characterized using current-voltage (I-V) curves with poled-up ($V_{max}=+3.0$ V) and -down ($V_{max}=-3.0$ V) PZT layers [Fig. 1(c)] [31]. The nonlinear behavior of both curves is consistent with the Brinkman model [3,25,32]: At a small voltage bias, the normalized differential conductance in the MFTJ [$G(V)/G(0), G=(dI/dV)$] can be described by a parabolical dependence of

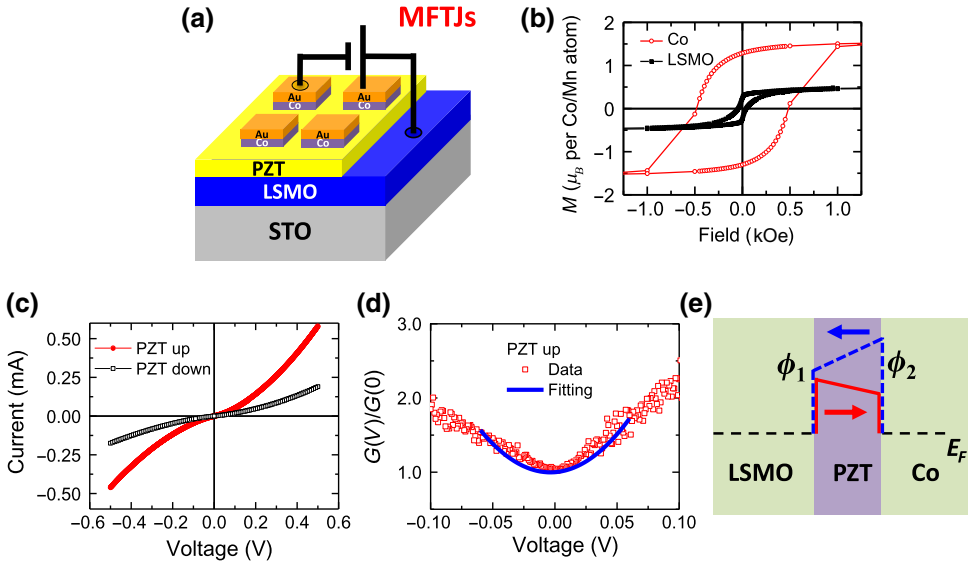

FIG. 1. Multiferroic tunnel junctions. (a) Schematic image of the LSMO/PZT/Co MFTJs. (b) Magnetic hysteresis loops of the LSMO and Co films used from FM electrodes with coercive fields of 40 and 500 Oe, respectively. (c) I-V curves of the junction (measured at 10 K and 2000 Oe) with the poled-up and -down PZT. (d) Dynamic conductance (red square dots, poled-up PZT) as a function of voltage calculated from the I-V curve and fitted by the Brinkman model (blue solid line) in small voltage range. (e) Energy diagram of the MFTJ with poled-up and -down PZT.

bias voltage (V), while neglecting high-order terms:

$$\frac{G(V)}{G(0)} = 1 - \frac{d\sqrt{2m_e}\Delta\phi}{12\hbar\bar{\phi}^{3/2}}V + \frac{d^2 m_e e}{4\hbar^2\bar{\phi}}V^2, \quad (1)$$

where d is the barrier thickness ($d = 5$ nm in this work); $\bar{\phi} = (1/2)(\phi_1 + \phi_2)$, i.e., the average barrier height at the LSMO/PZT (ϕ_1) and PZT/Co interface (ϕ_2); and $\Delta\phi = |\phi_2 - \phi_1|$ is the difference of asymmetric interfacial barriers. Figure 1(d) shows an example of $G(V)/G(0)$ from the I-V curve with poled-up PZT (scatters) and the Brinkman model fitting curve (the blue plot) from Eq. (1) using $\overline{\phi_\uparrow} = (1/2)(\phi_{\uparrow 1} + \phi_{\uparrow 2}) = 0.3$ eV and $\Delta\phi_\uparrow = |\phi_{\uparrow 2} - \Delta\phi_{\uparrow 1}| = 0.1$ eV. Thus, $\phi_{\uparrow 1} = 0.35$ eV and $\phi_{\uparrow 2} = 0.25$ eV can be estimated. Similarly, for poled-down PZT, we get $\overline{\phi_\downarrow} = (1/2)(\phi_{\downarrow 1} + \phi_{\downarrow 2}) = 0.5$ eV, $\Delta\phi_\downarrow = |\phi_{\downarrow 1} - \Delta\phi_{\downarrow 2}| = 0.2$ eV, and $\phi_{\downarrow 1} = 0.4$ eV, $\phi_{\downarrow 2} = 0.6$ eV, as illustrated by the schematic band structure in Fig. 1(e). The TER effect, which is defined as TER $= (R_\downarrow/R_\uparrow)$ (where $R_\uparrow$ and $R_\downarrow$ are the resistances of MFTJs if the PZT layer is fully poled up and down, respectively), can be expressed as [33,34]:

$$\mathrm{TER} \approx \exp\left(\frac{\sqrt{2m_e}}{\hbar}\frac{\Delta u}{\sqrt{u_0}}d\right), \quad (2)$$

where d is the thickness of the PZT; $\Delta u = \overline{\phi_\downarrow} - \overline{\phi_\uparrow}$, i.e., the barrier height changes upon reversal of the FE polarization; and u_0 is the potential barrier height of PZT, which can be determined as the average value of poled-up and -down states according to the Wentzel-Kramers-Brillouin approximation, i.e., $u_0 = (1/2)(\overline{\phi_\downarrow} + \overline{\phi_\uparrow})$.

B. TMR characterization in MFTJs and electrical modulation

The resistance of the MFTJ can also be tuned by an external magnetic. Figure 2 shows the multilevel resistance states of a MFTJ tuned by external magnetic and electric fields alternatively. The multistate measurements are conducted by first ramping the bias voltage to $V_{\max}$, to achieve one of the nonvolatile accumulated FE states [Fig. 2(c)], and then the voltage bias is reduced to V_{MR} ($|V_{\mathrm{MR}}| \le |V_{\max}|$) to probe the magnetoresistance of the MFTJ at this programmed FE state. By gradually tuning $V_{\max}$, the FE state of PZT can be accumulatively switched from the fully poled-up state, to the partially poled-down state, and then to the fully poled-down state [27]. By sweeping the magnetic field [Fig. 2(a)], TMR measurements are performed at each FE state [Fig. 2(d)]. The TMR value is calculated by

$$\mathrm{TMR} = \frac{R_{\mathrm{AP}} - R_{\mathrm{P}}}{R_{\mathrm{P}}} \times 100\%, \quad (3)$$

where R_{P} and R_{AP} are the resistances of the MFTJ device with parallel and antiparallel magnetic alignments of the FM electrodes, respectively.

(a) For $V_{\max} \ge +3.0$ V and $V_{\max} \le -3.0$ V, the R_{P} of the MFTJ remains unchanged by changing $V_{\max}$; this indicates that the two fully poled states are established. Remarkably, the polarity of the TMR response changes from negative to positive sign when the poling bias ($V_{\max}$) switches the FE polarization states of PZT from poled-up to poled-down states, which is consistent with a previous literature report [23].

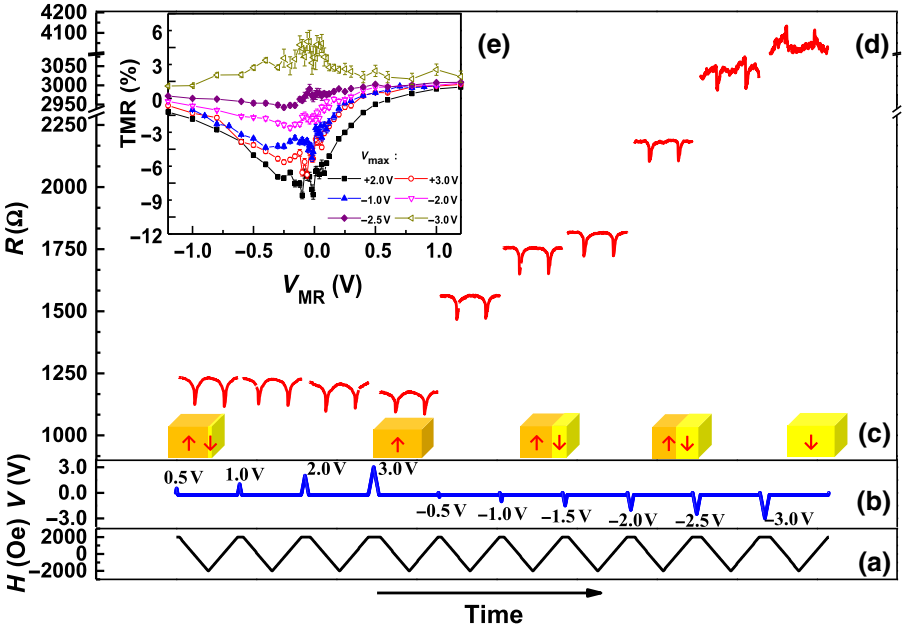

FIG. 2. Multilevel resistance states of the MFTJ tuned by external magnetic and electric fields. (a)–(d) Magnetic and electric field programing of resistance: the voltage is ramped to $V_{\max} = 0.5$, 1.0, 2.0, 3.0, −0.5, −1.0, −1.5, −2.0, −2.5, –3.0 V (b), to modulate the FE states of the PZT layer (c), and then to V_{MR} (=−0.25 V) for magnetoresistance measurements (d) by sweeping the magnetic field (a). (e) TMR as a function of V_{MR} measured after application of different $V_{\max}$.

(b) The change of R_P in the $-3.0\ \text{V} < V_{max} \leq 0\ \text{V}$ region corresponds to the formation of the mixed FE polarization state, with both poled-up and -down domains. TMR versus V_{MR} curves are plotted under different V_{max} in Fig. 2(e). A typical V_{MR} dependence with a peak TMR value around $V_{MR} = 0\,\text{V}$ is observed [35]. The bias voltage shifts the Fermi level of FM electrodes and their spin polarizations, and consequently modifies the TMR values, according to the Julliére model ($\text{TMR} = [2P_{LSMO}P_{Co}/(1 - P_{LSMO}P_{Co})]$) [36]. The quantitative dependence of TMR on V_{MR} depends on the spin-resolved band structure of the electrodes [35].

(c) For $0\ \text{V} \leq V_{max} < 3.0\ \text{V}$, the TMR is less sensitive to V_{max}, considering the measurement uncertainties while for $V_{max} < 0$ V, the sign of TMR changes dramatically from negative to positive [see Figs. 2(d) and 2(e)]. This can be understood as the FE domain in as-grown PZT films being naturally poled up, along the same direction of positive electric field ($V_{max} > 0$ V). A further increase in positive V_{max} does not change the FE polarization states significantly [27,28] nor the TER and TMR responses. In contrast, for $V_{max} < 0$ V, by gradually tuning the voltage level of V_{max}, the intermediate polarization states of PZT containing both FE poled-up and -down domains will be formed. Consequently, both TER and TMR change as a function of V_{max} until the fully FE poled-down state is reached.

C. Model and discussion

Figure 3 shows both measured and simulated TER responses in the MFTJ using a two-channel model upon V_{max} modulation. The TER response of MFTJs is derived from I-V characteristics, which strongly depend on V_{max} [Fig. 3(b)]. Considering two individual channels corresponding to the FE poled-up and -down domains, respectively, TER values can be defined as the ratio of device resistance with x(%) FE poled-down domains (R_x) to that of fully FE poled-up domains ($R_\uparrow$), i.e., $\text{TER}(x) \equiv (R_x/R_\uparrow)$. Here the device resistance (R_x) at an intermediate FE polarization state is expressed by

$$\frac{1}{R_x} = \frac{x}{R_\downarrow} + \frac{1-x}{R_\uparrow}, \tag{4}$$

$$x = \frac{\frac{R_\downarrow}{R_\uparrow}\left(1 - \frac{R_x}{R_\uparrow}\right)}{\frac{R_x}{R_\uparrow}\left(1 - \frac{R_\downarrow}{R_\uparrow}\right)} \times 100\%. \tag{5}$$

Taking the device resistance at $x = 0\%$ and at $x = 100\%$ as $R_\uparrow$ and $R_\downarrow$ respectively, x can be derived from the device resistance state, R_x, at each FE state, as shown in Fig. 3(c).

The fraction of switched FE poled-down domains as a function of V_{max} is plotted in Fig. 3(d). We find that the FE domain starts to switch at $V_{max} \leq -0.5$ V, where x changes dramatically from 0% to 100%. By fine-tuning the poling voltage, V_{max}, the fraction of the FE pole-down domain in the intermediate FE state can be electrically modulated, leading to gradual evolution of the device resistance.

The same parallel-resistor circuit model is also employed to interpret the evolution of the TMR response by switching the FE polarization of the PZT layer. Because of the antiparallel and parallel magnetic alignments of the two FM electrodes, there are two magnetic configurations at each FE state. Figures 4(a)–4(c) show the schematic magnetic configurations in MFTJs for the FE fully poled-up, partially poled-down, and fully poled-down states, respectively. Taking $V_{MR} = 0.2$ and -0.25 V as an example, the $R(H)$ curves at two FE fully pole states (i.e., $x = 0\%$ and $x = 100\%$) are presented in Figs. 4(d) and 4(e). The shape of the $R(H)$ hysteresis changes significantly when the PZT polarization is reversed; this suggests a change of the magnetic anisotropy of the Co layer or even the existence of exchange bias. This is probably caused by the migration of oxygen vacancies and formation of CoO at the PZT/Co interface when the PZT is poled down [37].

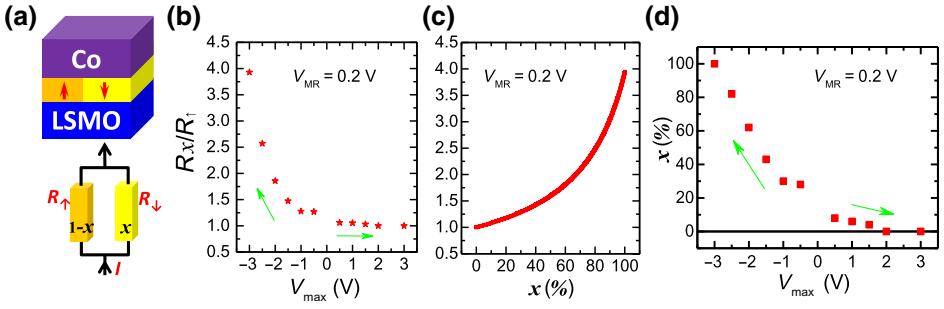

FIG. 3. Modulation and simulation of the TER of the MFTJ with an intermediate ferroelectric polarization state (x). (a) Schematics of the two-channel model consisting of pole-up and -down ferroelectric domains, which correspond to different resistivities. (b) TER defined as the resistance ratio, $R_x/R_\uparrow$, as a function of the poling voltage (V_{max}). (c) TER as a function of the fraction of FE pole-down domains (x) calculated from the two-channel model and maximum and minimum resistance values (see text). (d) The x value, as a function of V_{max}, extracted according to (b),(c). The arrows in (b),(d) indicate measurement sequence.

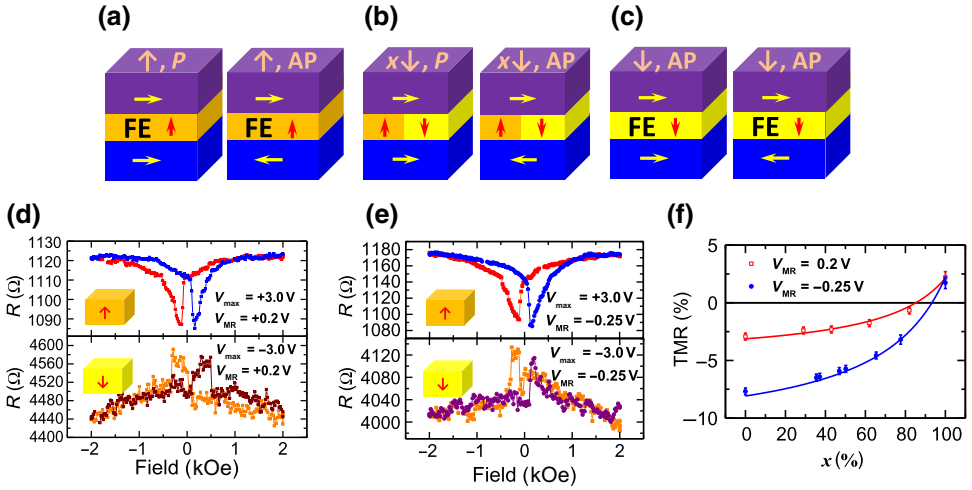

FIG. 4. Modulation and simulation of the TMR of the MFTJ with an intermediate ferroelectric polarization state (x). (a)–(c) Schematics of the MFTJ with magnetization of the ferromagnetic electrodes aligned parallel or antiparal and with the ferroelectric layer fully poled up ($x = 0\%$), partly poled down (x), or fully poled down ($x = 100\%$). (d) $R(H)$ of the MFTJ measured at $V_{MR} = 0.2$ V and (e) $V_{MR} = -0.25$ V for $x = 0\%$ [(a) state] and $x = 100\%$ [(c) state]. (f) Measured (scatters) TMR compared with TMR calculated (lines) from the two-channel model for $V_{MR} = 0.2$ V and $V_{MR} = -0.25$ V.

Taking the FE state into account, the TMR value of the MFTJ can be described as:

$$\mathrm{TMR} = \frac{R_{x,\mathrm{AP}} - R_{x,\mathrm{P}}}{R_{x,\mathrm{P}}} = \frac{R_{\downarrow,\mathrm{AP}} R_{\uparrow,\mathrm{AP}}}{R_{\downarrow,\mathrm{P}} R_{\uparrow,\mathrm{P}}} \times \frac{xR_{\uparrow,\mathrm{P}} + (1-x)R_{\downarrow,\mathrm{P}}}{xR_{\uparrow,\mathrm{AP}} + (1-x)R_{\downarrow,\mathrm{AP}}} - 1, \quad (6)$$

i.e., the TMR of intermediate FE states [Fig. 4(b)] can be estimated from the values of the two fully pole FE states [Figs. 4(a) and 4(c)]. The calculated results from Eq. (6) are presented in Fig. 4(f) for $V_{MR} = 0.2$ and -0.25 V, which agree well with the measured values and suggest the validity of the two-channel model.

IV. CONCLUSIONS

LSMO/PZT/Co-structured multiferroic tunnel junctions are fabricated, and the transport of spin-polarized charge carriers through the MFTJ via tunneling are successfully modulated using the electric-field-controllable ferroelectric states of the PZT layer. By fine-tuning the poling voltage, V_{max}, intermediate FE states are established, which lead to a gradual change of the TER and TMR responses of the device with multilevel resistance states, where the electric and magnetic fields serve as coarse and fine adjustments, respectively. Our work suggests a feasible approach to electrically tune the nonvolatile states of the FE layer, where both the TER and the TMR responses can be derived using a two-channel model corresponding to two FE domains. The electrically modulated intermediate FE polarization states in MFTJs can be used for multistate memory applications.

ACKNOWLEDGMENTS

This work was supported by the National Key Research and Development Program of China (2017YFB0305500), National Natural Science Foundation of China (11504055), the Hunan Provincial Natural Science Foundation of China (2018JJ2480), and Fundamental Research Funds of Central South University (2018zzts324). E.V. and D.S. are thankful for start-up support provided by North Carolina State University and a NC State-Nagoya Collaboration Grant. The sample synthesis work at ORNL is supported by the U.S. Department of Energy, Office of Science, Basic Energy Sciences, Materials Sciences and Engineering Division.

[1] S. Fusil, V. Garcia, A. Barthelemy, and M. Bibes, Magnetoelectric devices for spintronics, Annu. Rev. Mater. Res. **44**, 91 (2014).

[2] E. Y. Tsymbal and H. Kohlstedt, Tunneling across a ferroelectric, Science **313**, 181 (2006).

[3] W. F. Brinkman, R. C. Dynes, and J. M. Rowell, Tunneling conductance of asymmetrical barriers, J. Appl. Phys. **41**, 1915 (1970).

[4] J. P. Velev, J. D. Burton, M. Y. Zhuravlev, and E. Y. Tsymbal, Predictive modelling of ferroelectric tunnel junctions, NPG Comput. Mater. **2**, 16009 (2016).

[5] J. Tornos, et al., Ferroelectric Control of Interface Spin Filtering in Multiferroic Tunnel Junctions, Phys. Rev. Lett. **122**, 037601 (2019).

[6] H. Yamada, V. Garcia, S. Fusil, S. Boyn, M. Marinova, A. Gloter, S. Xavier, J. Grollier, E. Jacquet, C. Carretero, C. Deranlot, M. Bibes, and A. Barthelemy, Giant electroresistance of super-tetragonal $BiFeO_3$-based

ferroelectric tunnel junctions, Acs Nano **7**, 5385 (2013).

[7] Z. Wen, C. Li, D. Wu, A. Li, and N. Ming, Ferroelectric-field-effect-enhanced electroresistance in metal/ferroelectric/semiconductor tunnel junctions, Nat. Mater. **12**, 617 (2013).

[8] Z. Xi, J. Ruan, C. Li, C. Zheng, Z. Wen, J. Dai, A. Li, and D. Wu, Giant tunnelling electroresistance in metal/ferroelectric/semiconductor tunnel junctions by engineering the Schottky barrier, Nat. Commun. **8**, 15217 (2017).

[9] S. Dong, J.-M. Liu, S.-W. Cheong, and Z. Ren, Multiferroic materials and magnetoelectric physics: symmetry, entanglement, excitation, and topology, Adv. Phys. **64**, 519 (2015).

[10] G. Radaelli, D. Petti, E. Plekhanov, I. Fina, P. Torelli, B. R. Salles, M. Cantoni, C. Rinaldi, D. Gutiérrez, G. Panaccione, M. Varela, S. Picozzi, J. Fontcuberta, and R. Bertacco, Electric control of magnetism at the Fe/$BaTiO_3$ interface, Nat. Commun. **5**, 3404 (2014).

[11] H. J. Mao, P. X. Miao, J. Z. Cong, C. Song, B. Cui, J. J. Peng, F. Li, G. Y. Wang, Y. G. Zhao, Y. Sun, L. R. Xiao, and F. Pan, Interface-modification-enhanced tunnel electroresistance in multiferroic tunnel junctions, J. Appl. Phys. **116**, 053703 (2014).

[12] N. Jedrecy, H. J. von Bardeleben, V. Badjeck, D. Demaille, D. Stanescu, H. Magnan, and A. Barbier, Strong magnetoelectric coupling in multiferroic Co/$BaTiO_3$ thin films, Phys. Rev. B **88**, 121409(R) (2013).

[13] Y. Shirahata, R. Shiina, D. L. Gonzalez, K. J. A. Franke, E. Wada, M. Itoh, N. A. Pertsev, S. van Dijken, and T. Taniyama, Electric-field switching of perpendicularly magnetized multilayers, NPG Asia Mater. **7**, e198 (2015).

[14] V. Garcia, M. Bibes, L. Bocher, S. Valencia, F. Kronast, A. Crassous, X. Moya, S. Enouz-Vedrenne, A. Gloter, D. Imhoff, C. Deranlot, N. D. Mathur, S. Fusil, K. Bouzehouane, and A. Barthelemy, Ferroelectric control of spin polarization, Science **327**, 1106 (2010).

[15] M. Ghidini, R. Pellicelli, J. L. Prieto, X. Moya, J. Soussi, J. Briscoe, S. Dunn, and N. D. Mathur, Non-volatile electrically-driven repeatable magnetization reversal with no applied magnetic field, Nat. Commun. **4**, 1453 (2013).

[16] R. O. Cherifi, V. Ivanovskaya, L. C. Phillips, A. Zobelli, I. C. Infante, E. Jacquet, V. Garcia, S. Fusil, P. R. Briddon, N. Guiblin, A. Mougin, A. A. Uenal, F. Kronast, S. Valencia, B. Dkhil, A. Barthelemy, and M. Bibes, Electric-field control of magnetic order above room temperature, Nat. Mater. **13**, 345 (2014).

[17] Y. W. Yin, J. D. Burton, Y. M. Kim, A. Y. Borisevich, S. J. Pennycook, S. M. Yang, T. W. Noh, A. Gruverman, X. G. Li, E. Y. Tsymbal, and Q. Li, Enhanced tunnelling electroresistance effect due to a ferroelectrically induced phase transition at a magnetic complex oxide interface, Nat. Mater. **12**, 397 (2013).

[18] C. Song, B. Cui, F. Li, X. Zhou, and F. Pan, Recent progress in voltage control of magnetism: Materials, mechanisms, and performance, Prog. Mater. Sci. **87**, 33 (2017).

[19] J. M. Hu, L. Q. Chen, and C. W. Nan, Multiferroic heterostructures integrating ferroelectric and magnetic materials, Adv. Mater. **28**, 15 (2016).

[20] X. G. Wang, A. Sukhov, L. Chotorlishvili, C. L. Jia, G. H. Guo, and J. Berakdar, Electrically driven magnetic antenna based on multiferroic composites, J. Phys. Condens. Matter **29**, 095804 (2017).

[21] D. Pantel, H. Lu, S. Goetze, P. Werner, D. J. Kim, A. Gruverman, D. Hesse, and M. Alexe, Tunnel electroresistance in junctions with ultrathin ferroelectric $Pb(Zr_{0.2}Ti_{0.8})O_3$ barriers, Appl. Phys. Lett. **100**, 232902 (2012).

[22] A. Chen, Y. Wen, B. Fang, Y. Zhao, Q. Zhang, Y. Chang, P. Li, H. Wu, H. Huang, Y. Lu, Z. Zeng, J. Cai, X. Han, T. Wu, X. X. Zhang, and Y. Zhao, Giant nonvolatile manipulation of magnetoresistance in magnetic tunnel junctions by electric fields via magnetoelectric coupling, Nat. Commun. **10**, 243 (2019).

[23] D. Pantel, S. Goetze, D. Hesse, and M. Alexe, Reversible electrical switching of spin polarization in multiferroic tunnel junctions, Nat. Mater. **11**, 289 (2012).

[24] A. Chanthbouala, V. Garcia, R. O. Cherifi, K. Bouzehouane, S. Fusil, X. Moya, S. Xavier, H. Yamada, C. Deranlot, N. D. Mathur, M. Bibes, A. Barthélémy, and J. Grollier, A ferroelectric memristor, Nat. Mater. **11**, 860 (2012).

[25] A. Quindeau, I. Fina, X. Marti, G. Apachitei, P. Ferrer, C. Nicklin, E. Pippel, D. Hesse, and M. Alexe, Four-state ferroelectric spin-valve, Sci. Rep. **5**, 9749 (2015).

[26] A. Chanthbouala, A. Crassous, V. Garcia, K. Bouzehouane, S. Fusil, X. Moya, J. Allibe, B. Dlubak, J. Grollier, S. Xavier, C. Deranlot, A. Moshar, R. Proksch, N. D. Mathur, M. Bibes, and A. Barthelemy, Solid-state memories based on ferroelectric tunnel junctions, Nat. Nanotechnol. **7**, 101 (2012).

[27] D. Sun, M. Fang, X. Xu, L. Jiang, H. Guo, Y. Wang, W. Yang, L. Yin, P. C. Snijders, T. Z. Ward, Z. Gai, X. G. Zhang, H. N. Lee, and J. Shen, Active control of magnetoresistance of organic spin valves using ferroelectricity, Nat. Commun. **5**, 4396 (2014).

[28] L. Jiang, W. S. Choi, H. Jeen, T. Egami, and H. N. Lee, Strongly coupled phase transition in ferroelectric/correlated electron oxide heterostructures, Appl. Phys. Lett. **101**, 042902 (2012).

[29] H. N. Lee, S. M. Nakhmanson, M. F. Chisholm, H. M. Christen, K. M. Rabe, and D. Vanderbilt, Suppressed Dependence of Polarization on Epitaxial Strain in Highly Polar Ferroelectrics, Phys. Rev. Lett. **98**, 217602 (2007).

[30] I. Pintilie, C. M. Teodorescu, C. Ghica, C. Chirila, A. G. Boni, L. Hrib, I. Pasuk, R. Negrea, N. Apostol, and L. Pintilie, Polarization-control of the potential barrier at the electrode interfaces in epitaxial ferroelectric thin films, ACS Appl. Mater. Interfaces **6**, 2929 (2014).

[31] In our MFTJ, a ramping bias of $V_{MAX} = \pm 3.0$ V, with respect to the LSMO electrode, is used to ensure fully pole-up and -down PZT states. The poling voltage is higher than ∓ 0.8 V, with respect to that in the PFM tip, as expected, owing to a larger device area [27].

[32] W. Huang, Y. Lin, Y. Yin, L. Feng, D. Zhang, W. Zhao, Q. Li, and X. Li, Interfacial ion intermixing effect on four-resistance states in $La_{0.7}Sr_{0.3}MnO_3/BaTiO_3/La_{0.7}Sr_{0.3}MnO_3$ multiferroic tunnel junctions, ACS Appl. Mater. Interfaces **8**, 10422 (2016).

[33] J. G. Simmons, Generalized formula for the electric tunnel effect between similar electrodes separated

by a thin insulating film, J. Appl. Phys. **34**, 1793 (1963).

[34] A. Gruverman, D. Wu, H. Lu, Y. Wang, H. W. Jang, C. M. Folkman, M. Y. Zhuravlev, D. Felker, M. Rzchowski, C. B. Eom, and E. Y. Tsymbal, Tunneling electroresistance effect in ferroelectric tunnel junctions at the nanoscale, Nano Lett. **9**, 3539 (2009).

[35] J. M. De Teresa, A. Barthelemy, A. Fert, J. P. Contour, R. Lyonnet, F. Montaigne, P. Seneor, and A. Vaures, Inverse Tunnel Magnetoresistance in $Co/SrTiO_3/La_{0.7}Sr_{0.3}MnO_3$: New Ideas on Spin-Polarized Tunneling, Phys. Rev. Lett. **82**, 4288 (1999).

[36] M. Julliere, Tunneling between ferromagnetic films, Phys. Lett. A **54**, 225 (1975).

[37] K. Zhang, Y.-l. Cao, Y.-w. Fang, Q. Li, J. Zhang, C.-g. Duan, S.-s. Yan, Y.-f. Tian, R. Huang, R.-k. Zheng, S.-s. Kang, Y.-x. Chen, G.-l. Liu, and L.-m. Mei, Electrical control of memristance and magnetoresistance in oxide magnetic tunnel junctions, Nanoscale **7**, 6334 (2015).